BOLLETTINO DI GEOFISICA TEORICA ED APPLICATA VOL. 44, N. 3-4, PP. 281-305; SEP.-DEC. 2003

Ray tracing applied to travel time seismic tomography: theory and examples

E. CARDARELLI

Dipartimento di Idraulica, Trasporti e Strade, Università degli Studi di Roma, Italy

(Received, June 10, 2002; accepted November 22, 2002)

Abstract - This paper is a short review of recent methods of ray tracing with particular regard to the ones used in seismic transmission tomography. Some aspects are described with their main characteristics and drawbacks. The main aspects of Linear Traveltime Interpolation algorithm and its implementation is described in the case of a transversely isotropic medium also by the results of a synthetic model. Covariance matrices are used as a tool for the choice of the grid distribution of the investigated area. Some particular features are discussed and two case histories are shown considering both the cases of isotropic and transversely isotropic medium.

1. Introduction

Ray tracing approaches, to evaluate the path of the seismic ray, were developed by many authors (Bois et al., 1971; Cerveny et al., 1977; Julian and Gubbins, 1977; Lytle and Dines, 1980; Vidale, 1988, 1990; Saito, 1989, 1990; Moser, 1991; Asakawa and Kawanaka, 1993). In the last few years, ray tracing techniques were applied in seismic tomography to evaluate the field velocity of the investigated area. Generally, the tomographic technique considers a 2D cell section where a constant velocity is assumed in each cell. Because the conventional ray tracing approaches are difficult to apply to cell model structures, new techniques were developed for isotropic (Vidale, 1988, 1990; Moser, 1991; Matsuoka and Ezaka, 1992; Asakawa and Kawanaka, 1993) and anisotropic (Cerveny, 1972; Chapman and Pratt, 1992; Pratt and Chapman, 1992; Faria and Stoffa, 1994) models.

Conventional methods like bending and shooting, show drawbacks in the case of high contrast velocities in grid or cell models of the investigated area.

Corresponding author: E. Cardarelli, Dipartimento di Idraulica, Trasporti e Strade, Università degli Studi di Roma "La Sapienza", Via Eudossiana 18, 00184 Roma, Italy. Phone: +39 0644585079; e-mail: ettore.cardarelli@uniroma1.it

The shooting method uses the given initial position and direction of ray to converge to a desired position (Bois et al., 1971; Julian and Gubbins, 1977). The source position is taken as an initial point then the rays are shot from this point under different angles α_i. An iterative loop is used to find the ray that crosses the geophone location.

When shooting is applied to a cell structure model it has many disadvantages as follows:

1. head waves are not generally included; because paths of rays are assumed first, an infinite number of paths have to be considered if we are going to take into account head waves;
2. one path is generally assumed for each source and receiver; in this method, it is difficult to deal with multi-path problems because the path is calculated according to a shooting angle; when direct and head waves arrive simultaneously, we have to consider both such waves. In a tomographic analysis these two paths give us two independent equations which should be used to invert travel times;
3. in a cell model, a large computation time is required; the shooting method depends on the boundary that the ray has to cross during the travel from the source to the receiver;
4. for a complicated velocity structure it is difficult to find the path.

The bending method (Wesson, 1971) on the other hand does not use the initial direction of the ray but the path is guessed between the two end points, then is perturbed iteratively so as to satisfy the appropriate differential equations, or the Fermat' principle directly.

The simpler, starting model is to consider the average value of the velocity field calculated from the measured travel time and distances between sources and sensors. In this case, the rays are straight during the first iteration. On succeeding iterations, the rays are curved and are compared with those of the previous iteration, to detect the amount of change, if the ray is changing we would continue the inversion procedure. If the rays are stabilised, the inversion is taken to the best approximation. In the simpler velocity model the bending method is usually more efficient than the shooting method. When the velocity structure is more complicated, efficiency of the bending is lower and has a tendency to overlook some multiple rays (Cerveny, 1987), furthermore, is not clear if the minimal is local or global.

For these reasons, and to overcome some of the difficulties mentioned above, other techniques were developed. The first approach is the Huygens' principle method (Saito, 1990; Moser, 1991). The second approach is based on solving the eikonal equation using the Finite Differences Method (FDM); this method was proposed by Vidale (1988). He considered two steps: in the forward step the computation of traveltimes from the source to a particular point (grid points) throughout the investigated area; and, in the backward step, the best estimation of the ray paths from the traveltime data obtained in the first step. This approach has the great advantage that the techniques used in each step can be different (Matsuoka and Ezaka, 1992).

The Linear Traveltime Interpolation method (LTI) is such a technique. It was introduced by Asakawa and Kawanaka (1993) who assumed that the traveltime at any point along the cell boundary can be interpolated linearly between the traveltimes at adjacent discrete points on the same cell boundary. They demonstrated this method to be more accurate and stable than FDM.

Li and Ulrych (1993) provided two different formulations of the LTI method, and demonstrated that in the near field the accuracy of traveltime computation is improved with respect to the Vidale (1988) formula.

The LTI method is especially suitable for seismic travel time tomography. In fact, ray paths are determined by the calculation points (or grid points) located on the cell boundary thus, according to the hypothesis of constant velocity in each cell, the ray paths are represented by segments that change in direction at the cell boundary.

2. Background and LTI implementation in transversely anisotropic media

The LTI method starts from the consideration that the minimum travel time from the source S and the receiver R can be calculated starting from the Fermat principle and from the linear interpolation between two points of the grid in which the times have been calculated.

For the complete theory of the LTI method, we refer to Appendix A and to the paper of Asakawa and Kawanaka (1993).

We implemented the method considering anisotropic media in the simple case of an elliptical model under the hypothesis that one of the two main anisotropic directions coincide with one of the directions of the frame (Cardarelli and Cerreto, 2002). If we define the slowness of the two main directions with S_x and S_z and with ϕ, the angle by which the slowness $S(\phi)$ is evaluated (Postma, 1955; Levin, 1978) we can write:

$$S^2(\phi) = S_z^2 \cos^2\phi + S_x^2 \sin^2\phi. \quad (1)$$

The procedure we used, in the case of elliptical anisotropic media, is not different from the procedure indicated by Asakawa and Kawanaka (1993) in the case of isotropic material. The authors suggest evaluating the path proceeding column by column and if necessary to repeat the calculation row by row. Considering that in seismic 2D tomography for building structures, sources and receivers are arranged along the whole boundary of the investigated object (ray coverage 360°) refraction at a critical angle must be considered throughout the whole boundary of the cells. For this reason, to simplify the procedure, we repeat the calculus column by column twice just swapping the *X* axis with *Z* axis and vice versa.

The complete formulation for the implementation of LTI in the case of elliptical anisotropic media is reported in Appendix B.

Because the rays are forcibly refracted on a priori fixed surfaces defined by the grid geometry and as the matrix to be inverted depends on grid choice, not being able to vary the cell spacing leads to risk of losing all the advantage of ray tracing. Furthermore, because dimensions of cells determine the size of the minimum detected anomaly, it is of paramount importance to consider the Fresnel ray theory.

If we indicate the minimum dimensions of the cells with r_{min} we can calculate by the $r_{min} = \frac{1}{2}\sqrt{\frac{Lv}{f}}$ where L is the distance between the source and the receiver, v the mean velocity of the medium and f the dominant frequency of the signal. In the case of anisotropic models both velocities of main directions of anisotropy were considered to calculate the minimum dimensions of cells.

The ray tracing algorithm was included in a procedure of calculus of anisotropic seismic transmission tomography. We choose the algorithm proposed by Michelena et al. (1993) in which the travel-time is given by:

$$t_i(s) = \sum_{j=1}^{N} \sqrt{\Delta x_{ij}^2 \, S_j^2 + \Delta z_{ij}^2 \, S_{j+N}^2}, \tag{2}$$

where S_j is slowness in one of the two main directions of anisotropy, S_{j+N} slowness in the perpendicular one, Δx and Δz are the components of the ray path in the corresponding directions, and N is the number of the cells. To invert the data we used the Coniugate Gradient (CG) algorithm (Press et al., 1992). The system was preconditioned by using damping factors in accordance with $(J^T J + W)\ \Delta S = J^T\ \Delta t$; here W is the diagonal matrix of damping factors, J the Jacobian solution matrix; $\Delta S = (S_{n+1} - S_n)$ and $\Delta t = t_m - t(S_n)$, where S_n, t_m and $t(S_n)$ are respectively the vector of unknowns, the vector of measured times and the vector of calculated times (Cardarelli and de Nardis, 2001). In the above the $n + 1$ index indicates the actual step, the n index the previous one and the m index the mth traveltime of data set.

The procedure applied is as follows (Fig.1):

1. compute travel times in the given model, (in the first step the velocities are guessed) calculate the matrix J and find the residual;
2. approximate the solution of the linear problem by applying few CG iterations;
3. smooth the updated slowness model;
4. update the paths considering the new inversion results;
5. repeat the previous steps until there is no reduction in the data misfit.

The procedure is summarised by the flowchart in Fig.1.

3. Synthetic tests

To evaluate algorithm performances, a synthetic test was carried out. A square model 7x7 m with elliptical anisotropic characteristics was created (Figs. 2a and 2b). A summary of the test is reported here, the complete test is reported in the paper by Cardarelli and Cerreto (2002). Considering the same data set (traveltimes) two other different distributions of geometry cells were tested (grid#1 and grid#2) to evaluate if this parameter is critical for the inversion (Figs. 2c and 2d). Because head waves arise on the boundary of the cells the lengths of paths of the rays are determined by such a choice. The results of such a test are summarised in Tables 1 to 3. Observing Tables 2 and 3, it is possible to note that the particular distribution of cell grid geometry, influences the solution quite strongly when ray tracing is used, whereas the sensitivity is far less when the rays are assumed to be straight lines. This is evident in the case of grid #2 (Fig. 2d), where the V_x field is solved better in the straight ray approximation than ray tracing approximation.

For a better understanding of how both grid choice and successive iterations influence

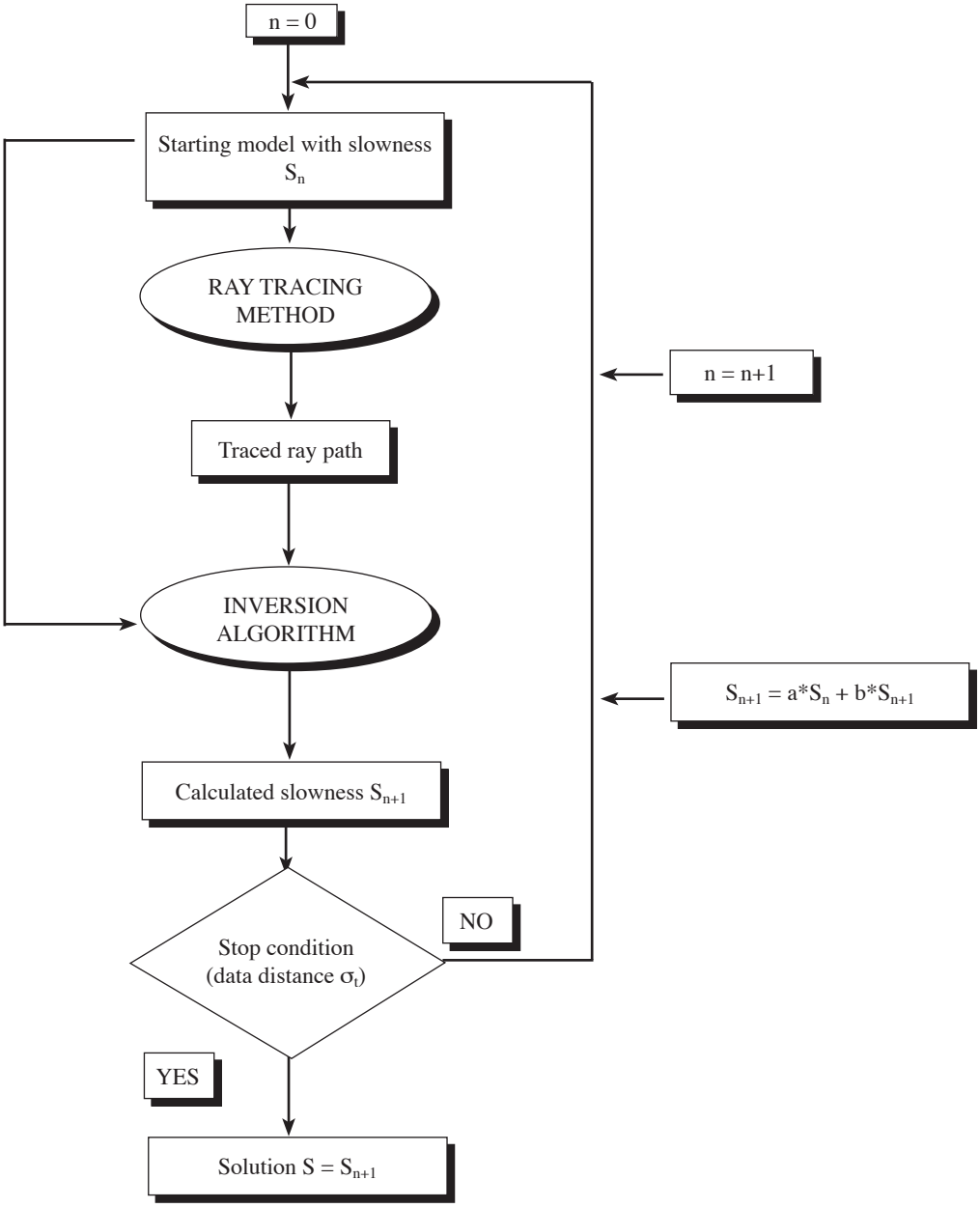

Fig. 1 - Flow chart of the inversion and raytracing procedure (after Cardarelli and Cerreto, 2002).

the inversion results (as the Jacobian matrix changes at each iteration and consequently the ray coverage of cells), a study on covariance matrices (Menke, 1989; Cardarelli, 2000) was performed. If we indicate with G the matrix in which the elements g_{ij} correspond to the ith ray in the jth cell with G^T the transpose of G and with β the dumping factor under the hypothesis of uncorrelated data the unit covariance matrix (UCM) is defined as:

$$Cov = (G^T G)^{-1} G^T G (G^T G)^{-1} = (G^T G)^{-1},$$

with dumping we obtain (Aki and Lee, 1976):

$$Cov = (G^T G + \beta I)^{-1} G^T G (G^T G + \beta I)^{-1} = (G^T G + \beta I)^{-1} R^T,$$

where R is the Data Resolution Matrix defined as:

$$R = (G^T G + \beta I)^{-1} G^T G.$$

In the case of elliptical anisotropy in each cell the two components of the rays in the directions of the two main components of anisotropy have to be considered. For this reason if the ray travels, for example, mainly in X direction the ray coverage in this direction will be better than in the Z direction and consequently the V_x velocity field will be solved better than V_z field (Fig. 3). To evaluate such a point and to improve inversion results UCM is a useful tool.

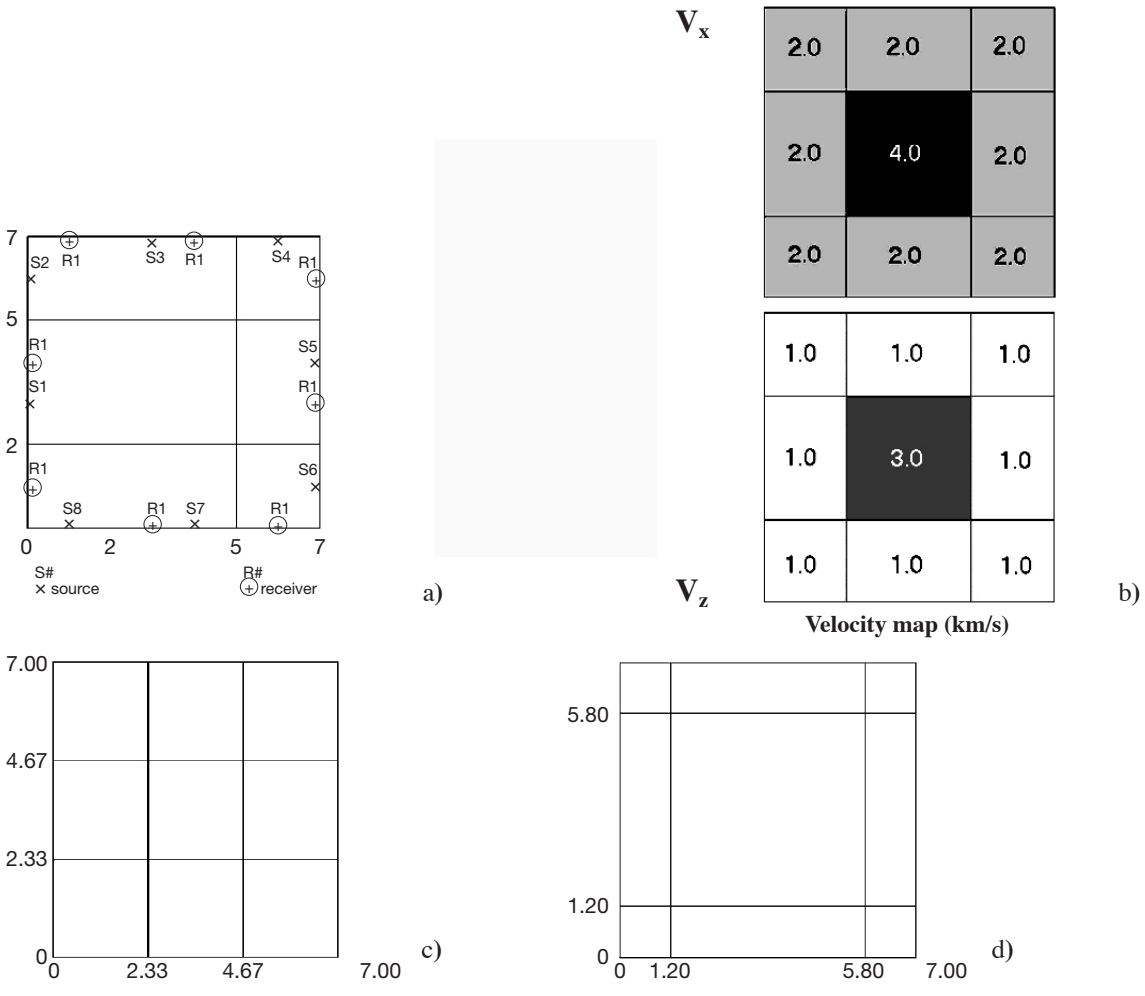

Fig. 2 - Cell identification in grid models of synthetic test: a) grid that fits the model exactly; b) velocity fields of main directions of anisotropy; c) grid#1 in which all the cells have the same dimensions; d) grid#2 in which the inner cell has the biggest dimensions.

Table 1 - Comparison between results obtained by the two methods when inverting synthetic data with noise, grid fits the model exactly. Test: data with noise and grid fitting the model exactly. Average measured time: 3.12 ms; Average V_X = 2.22 km/s; Average V_Z = 1.22 km/s.

	σ_t (ms)	% of average time	σ_{V_X} (km/s)	% of average V_X	σ_{V_Z} (km/s)	% of average V_Z
straight ray path	0.315	10.1	0.992	44.7	0.415	34.0
ray tracing	0.165	5.3	0.170	7.7	0.107	8.8

Table 2 - Comparison between results obtained by the two methods when inverting synthetic data with noise and grid#1.Test: data with noise and grid #1. Average measured time: 3.12 ms; Average V_X = 2.22 km/s; Average V_Z = 1.22 km/s.

	σ_t (ms)	% of average time	σ_{V_X} (km/s)	% of average V_X	σ_{V_Z} (km/s)	% of average V_Z
straight ray path	0.345	11.1	0.682	30.7	0.558	45.7
ray tracing	0.245	7.9	0.335	15.1	0.196	16.1

Table 3 - Comparison between results obtained by the two methods when inverting synthetic data with noise and grid#2. Test: data with noise and grid #2. Average measured time: 3.12 ms; Average V_X = 2.22 km/s; Average V_Z = 1.22 km/s.

	σ_t (ms)	% of average time	σ_{V_X} (km/s)	% of average V_X	σ_{V_Z} (km/s)	% of average V_Z
straight ray path	0.298	9.6	0.392	17.7	0.468	38.4
ray tracing	0.230	7.4	0.479	21.6	0.341	28

The covariance matrix of both velocity fields was calculated at the same time and then the diagonal elements of these matrices were located on the corresponding cells. In such a way, it was possible to understand, directly, where data errors are more amplified.

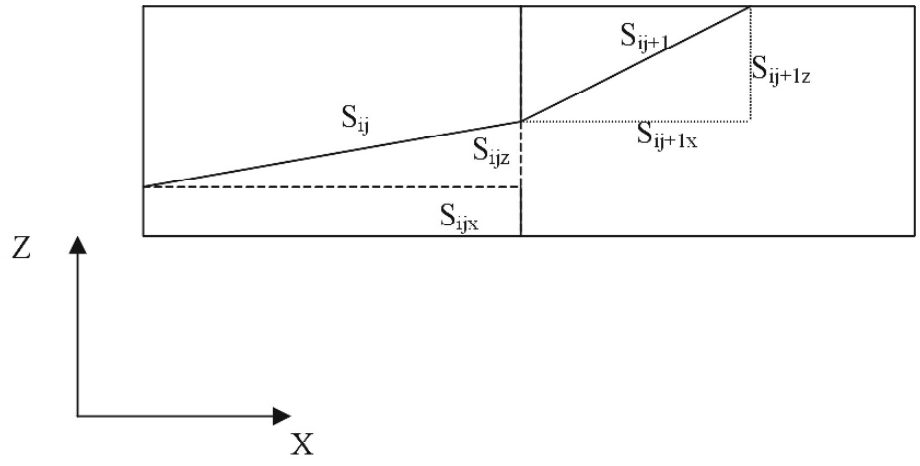

Fig. 3 - Example of ray coverage depending on the components of the ray.

In Figs. 4, 5 and 6, the covariance matrices of the three different grid geometries of the synthetic test are represented. In Fig. 4a the values of the UCM of the first iteration of the inversion procedure of the model with a grid that fits the model exactly is shown. In Figs. 4b and 4c, the elements of the main diagonal of both main directions of anisotropy are located in the respective cells; in Fig. 4f, the UCM of the last iteration of the inversion and in Figs. 4d and 4e the elements of the main diagonal of both main directions. Comparing the values of these matrices with the analogous ones of Figs. 5 and 6, that represent the UCM of grid #1 and grid #2, it can be noted that the results are analogous to those summarised in the Tables 1 to 3. In fact, the higher values of the main diagonal of UCM are those that correspond to grid #2 that has the higher values of model and data distance. It means the choice of this grid is the worst, with respect to the others. Furthermore, analysing Figs. 4e, 4f and the analogous 5e, 5f and 6e and 6f, it is possible to detect the cells in which the error can be amplified more with respect to the others. It is possible to confirm such results following the ray tracing of Figs. 4d and 4h and the analogous one of Figs. 5d and 5h and Figs. 6d and 6h.

4. Two case histories

To summarise, and to better understand the previous sections, two examples of seismic tomography are shown. In both examples, ray tracing and straight ray path approximations were used. In the first example, an elliptical anisotropic model was considered, in the second, an example of an isotropic model. Covariance matrices were calculated in both examples.

4.1. First example: seismic anisotropic tomography on an ancient monument

This survey (Cardarelli and de Nardis, 2001; Cardarelli and Cerreto, 2002) was carried out to investigate the decay degree of two columns of the Antonino and Faustina temple in the Roman Forum in Rome, and consequently to redirect the restorer during the restoration. The columns have a diameter of 1.5 m and are 15 m long, they are formed of cipollino marble that is made up of calcite interbedded with mica. The data acquisition procedure and data processing of the whole survey are referred in the papers of Cardarelli and de Nardis (2001) and Cardarelli and Cerreto (2002).

At first isotropic model was considered with a linear ray path, then elliptical anisotropy was considered with ray tracing. The results of a section of column C are shown in Fig. 7. In Fig. 7a straight rays were considered whilst in Fig. 7b ray tracing with cells with variable dimensions were introduced. Analysing the figure, it is possible to note that in the case of ray tracing a higher resolution of velocity fields and lower data distance are reached. In Fig. 8, both coverage of straight ray (Fig. 8a) and last iteration of ray tracing (Fig. 8b) is shown, it is evident in Fig. 8b that the rays travel in the middle side of the section where the velocity is higher. In this case, it is interesting to analyse the covariance matrix (Fig. 9c) of the last iteration of the inversion procedure to detect the cells with higher amplification of data error. In Figs. 9a and 9b the values

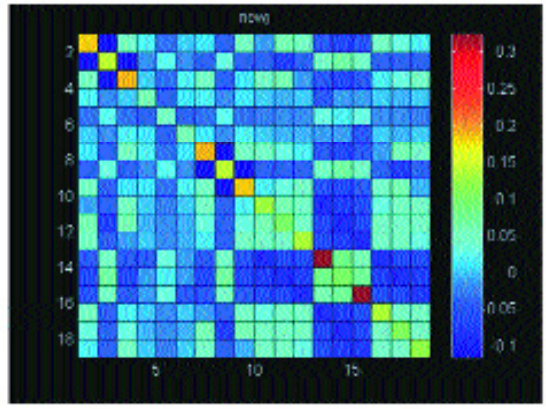

a)

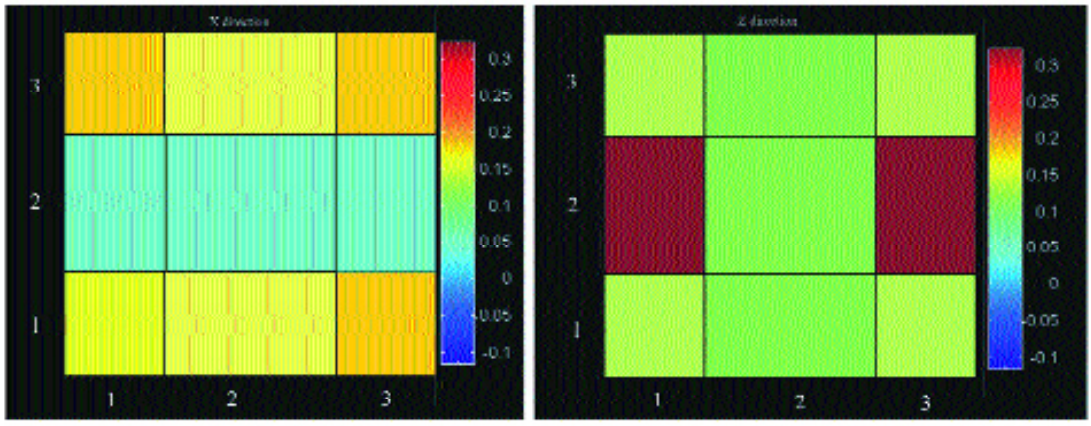

b) c)

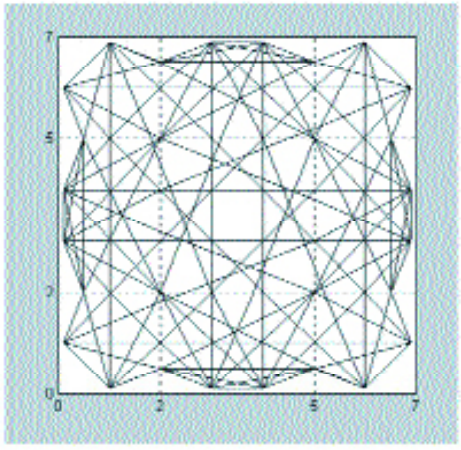

d)

Fig. 4 - a) UCM of the first iteration of the model that fits the data set exactly, b) and c) location of the values of the main diagonal of the UCM of the first iteration of the model that fits the data set exactly, d) ray tracing of the first iteration of the model that fits the data set exactly e) UCM of the last iteration of the model that fits the data set exactly, f) and g) location of the values of the main diagonal of the UCM of the last iteration of the model that fits the data set exactly h) ray tracing of the last iteration of the model that fits the data set exactly.

e)

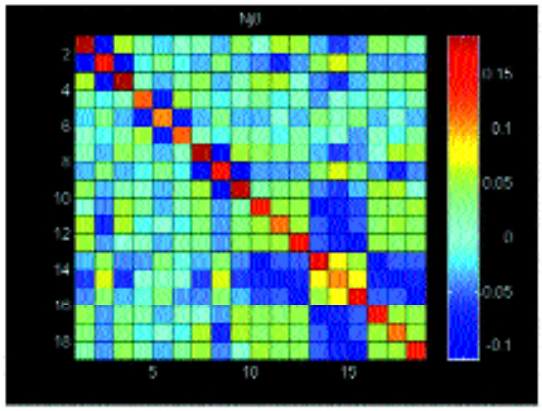

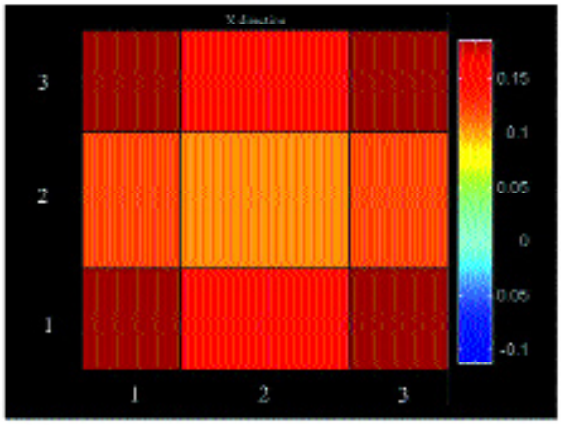

f)

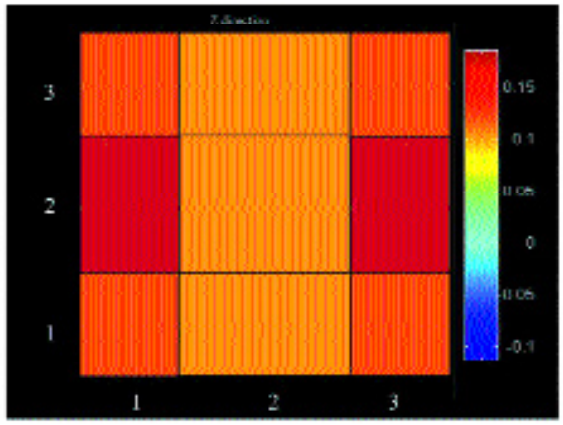

g)

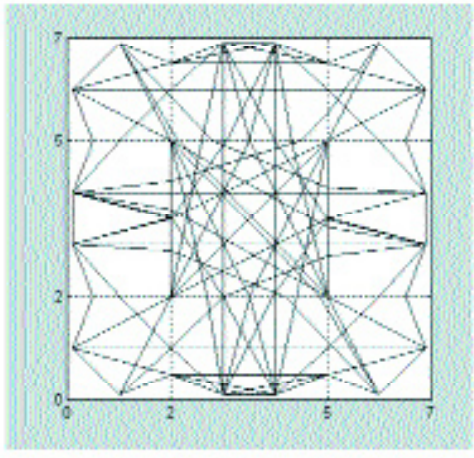

h)

Fig. 4 - continued.

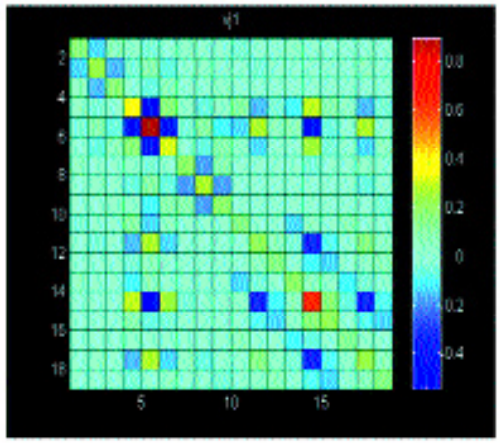

a)

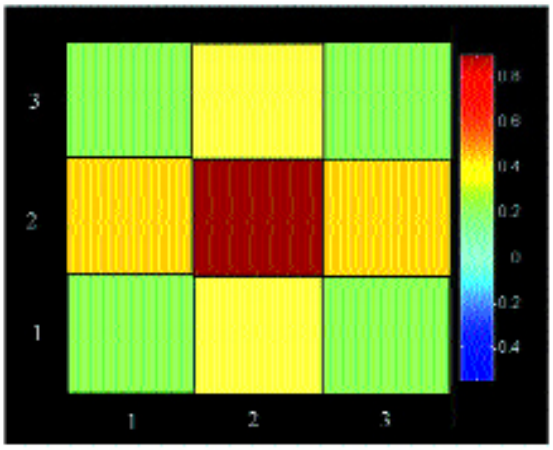

b)

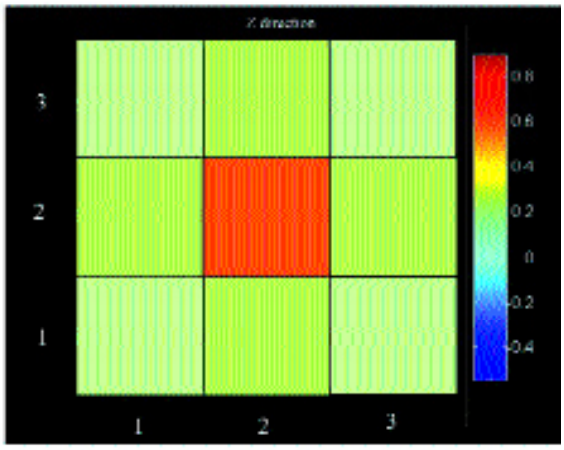

c)

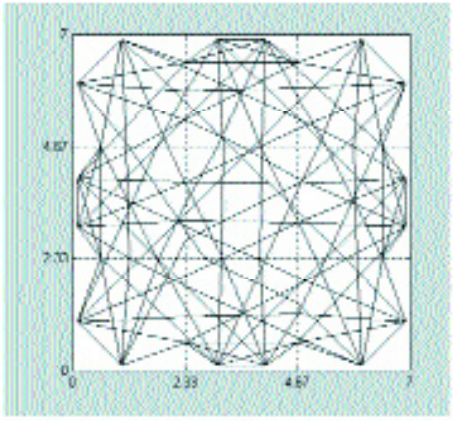

d)

Fig. 5 - a) UCM of the first iteration of the grid#1, b) and c) location of the values of the main diagonal of the UCM of grid#1, d) ray tracing of the first iteration of grid#1, e) UCM of the last iteration of grid#1, f) and g) location of the values of the main diagonal of the UCM of the last iteration of grid#1, h) ray tracing of the last iteration of grid#1.

e)

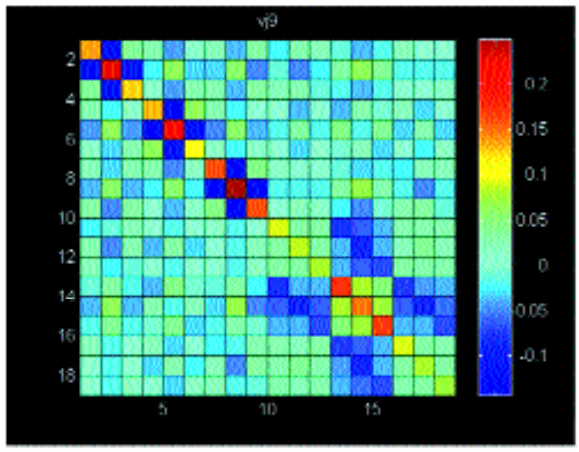

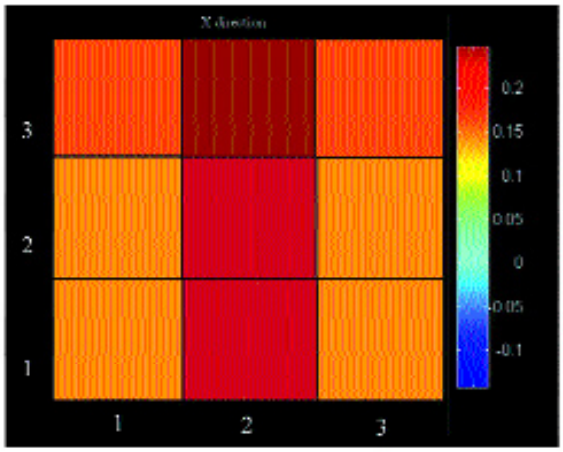

f)

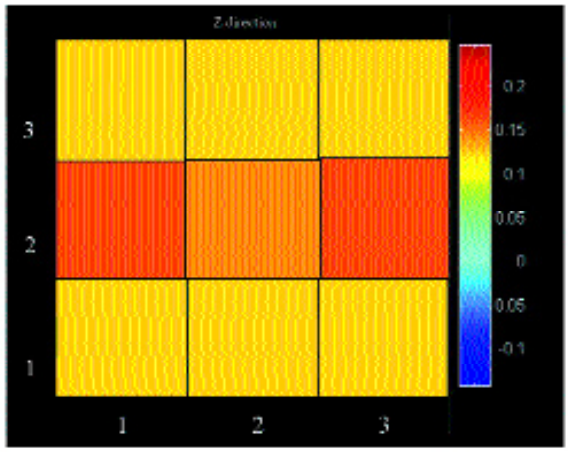

g)

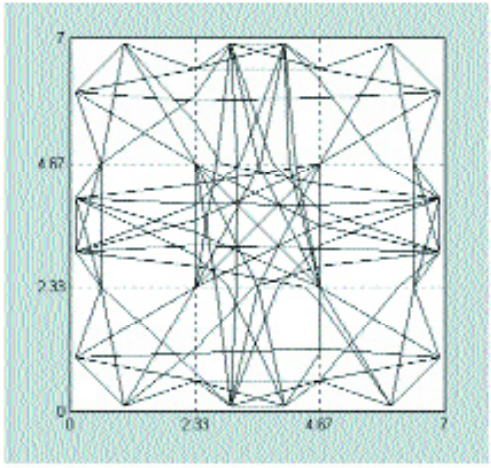

h)

Fig. 5 - continued.

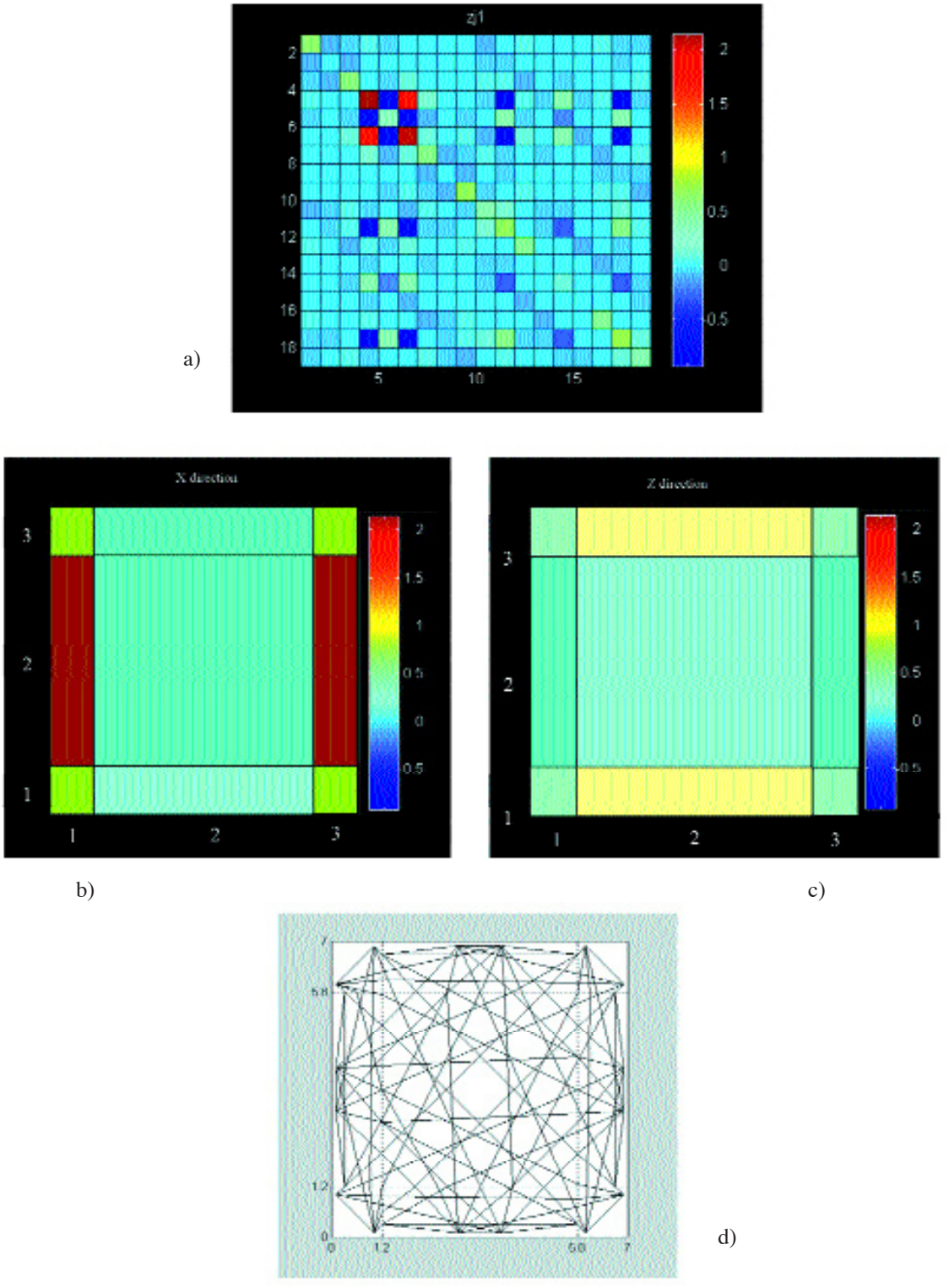

Fig. 6 - UCM of the first iteration of grid#2, b) and c) location of the values of the main diagonal of the UCM of grid#2, d) ray tracing of the first iteration of grid#2, e) UCM of the last iteration of grid#2, f) and g) location of the values of the main diagonal of the UCM of the last iteration of grid#2, h) ray tracing of the last iteration of grid#2.

e)

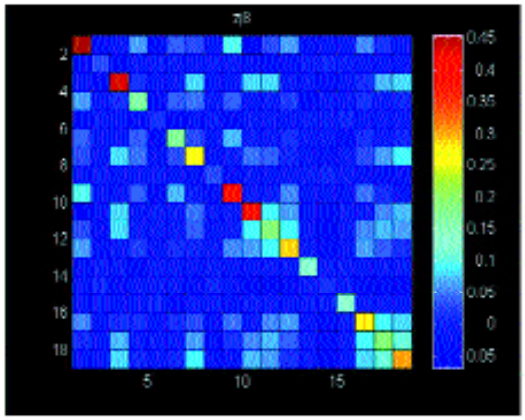

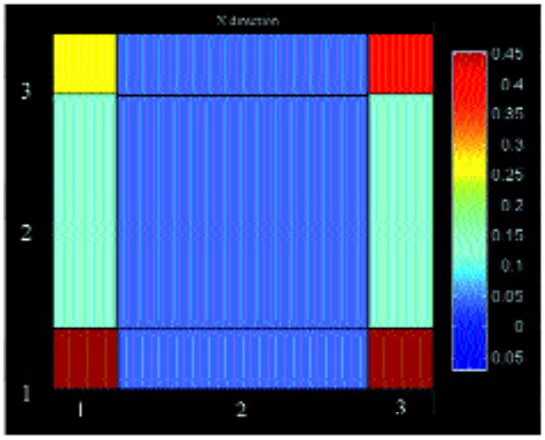

f)

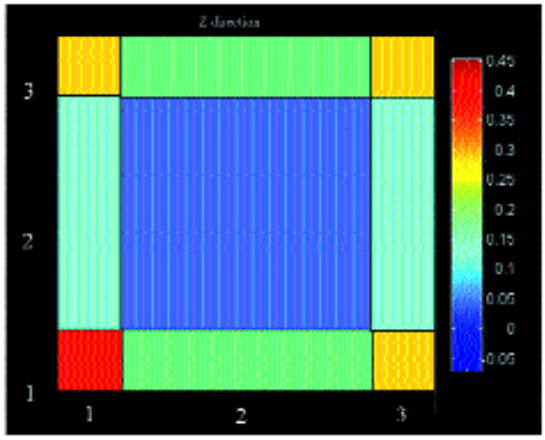

g)

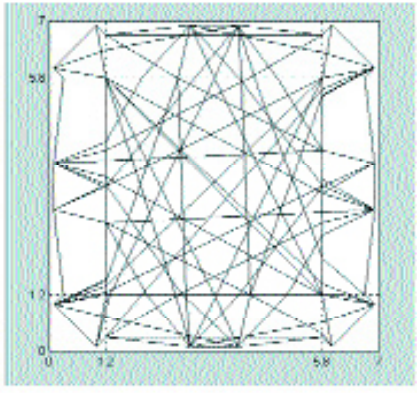

h)

Fig. 6 - continued.

of the main diagonal are located on the cell model for a better understanding of the results. The different values of the covariance matrices arise, because in the case of an elliptical anisotropic model, as we described in the previous paragraph, we have to consider the rays as the sum of the two components that correspond to the main directions of anisotropy.

In Fig. 9a, the coefficients of the main diagonal of the covariance matrix of X direction, that represents the higher velocity field, are located. In this figure, it is evident that the inner cells are better conditioned, this is because the inner side is characterised by high velocity and the rays, obeying the Fermat principle, cross the inner cells in the X direction to reach the sensors, performing a good coverage of such cells. On the contrary, in the Z direction, that represents the

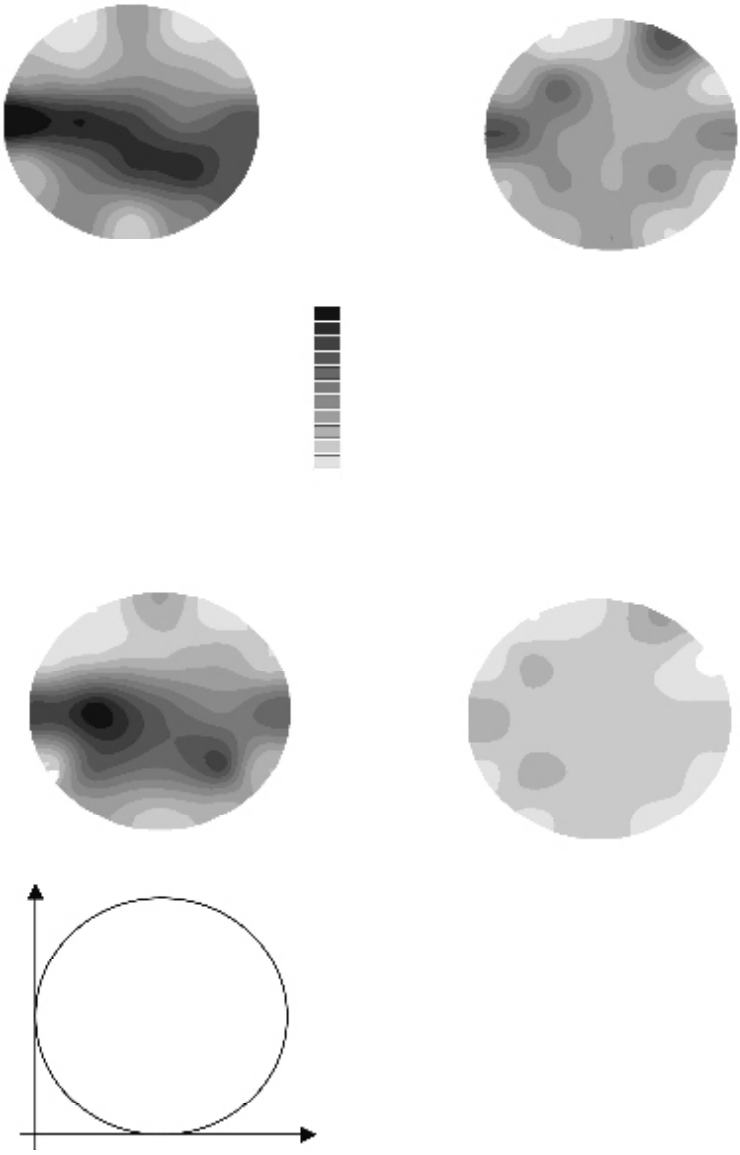

Fig. 7 - Seismic tomography results: a) linear ray path approximation and cells of varying size, b) ray tracing and cells of varying size (after Cardarelli and Cerreto, 2002).

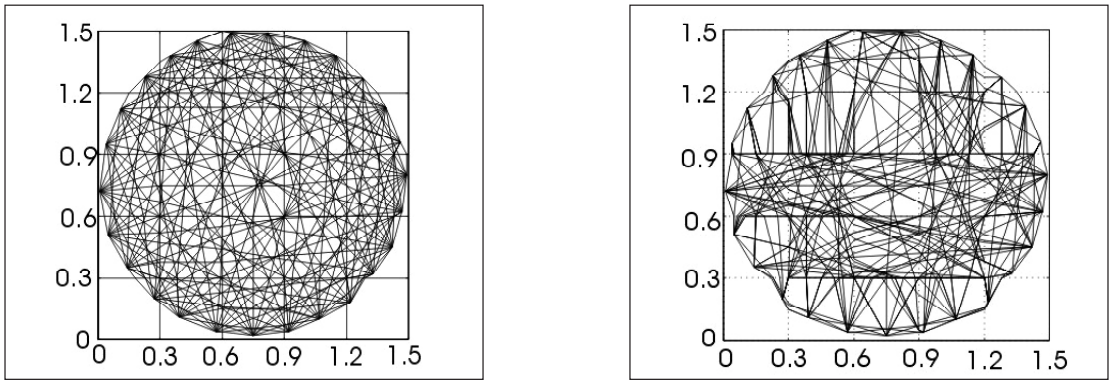

Fig. 8 - Traced ray path in elliptical anisotropic medium: a) linear ray path approximation; b) rays traced in a heterogeneous medium modelled by a grid with cells of variable size (after Cardarelli and Cerreto, 2002).

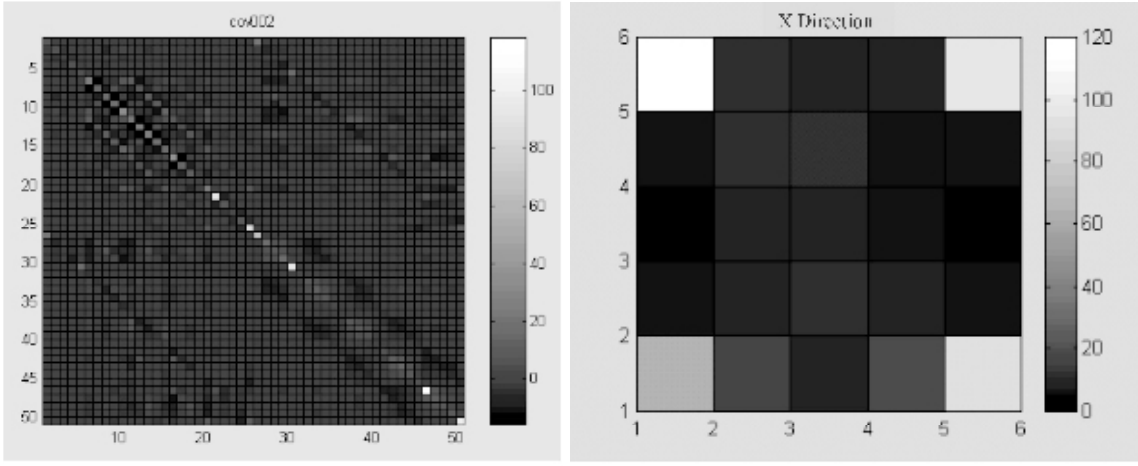

a) b)

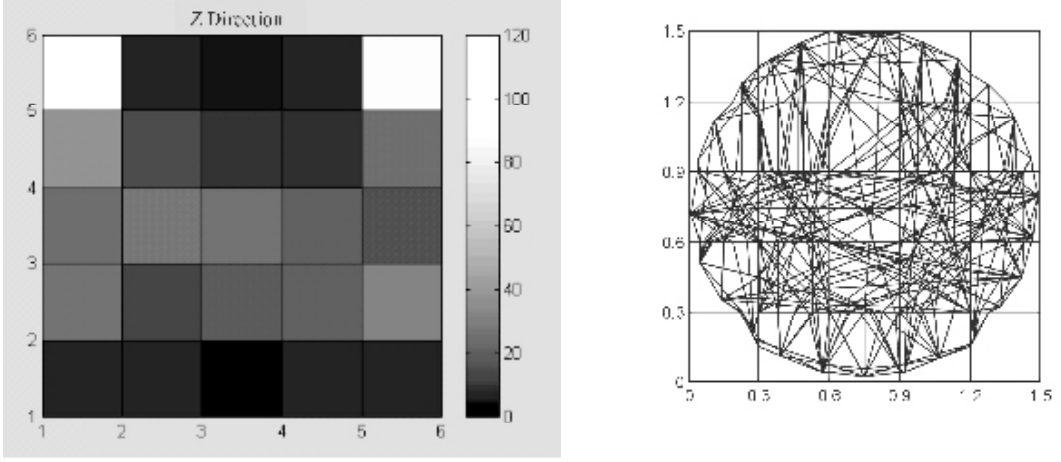

c) d)

Fig. 9 - a) UCM of the last step of the seismic anisotropic inversion, b) and c) location of the values of the main diagonal of the UCM of the last step, d) rays traced in a heterogeneous medium modelled by a grid with cells of variable size.

lower velocity field, the rays cross the lower velocity superficial cells with the minimum path, that in this case coincides with the Z direction, for this reason a good coverage of such cells is performed in Fig. 9b. For a better understanding ray tracing, please see Fig.9d.

4.2. Second example: seismic isotropic tomography in S. Nicolò all'Arena (CT)

This survey was performed in the church of S. Nicolò all'Arena at Catania Sicily, to test some massive stone pillars. The section of the pillars is about 16 m^2, they are built with volcanic stones and lime mortar. The survey consists in 28 tomographic sections. For each section, 23 sensors and 21 shot points were located around the investigated pillar; the data were inverted with different algorithms depending if straight ray paths or ray tracing was considered. The

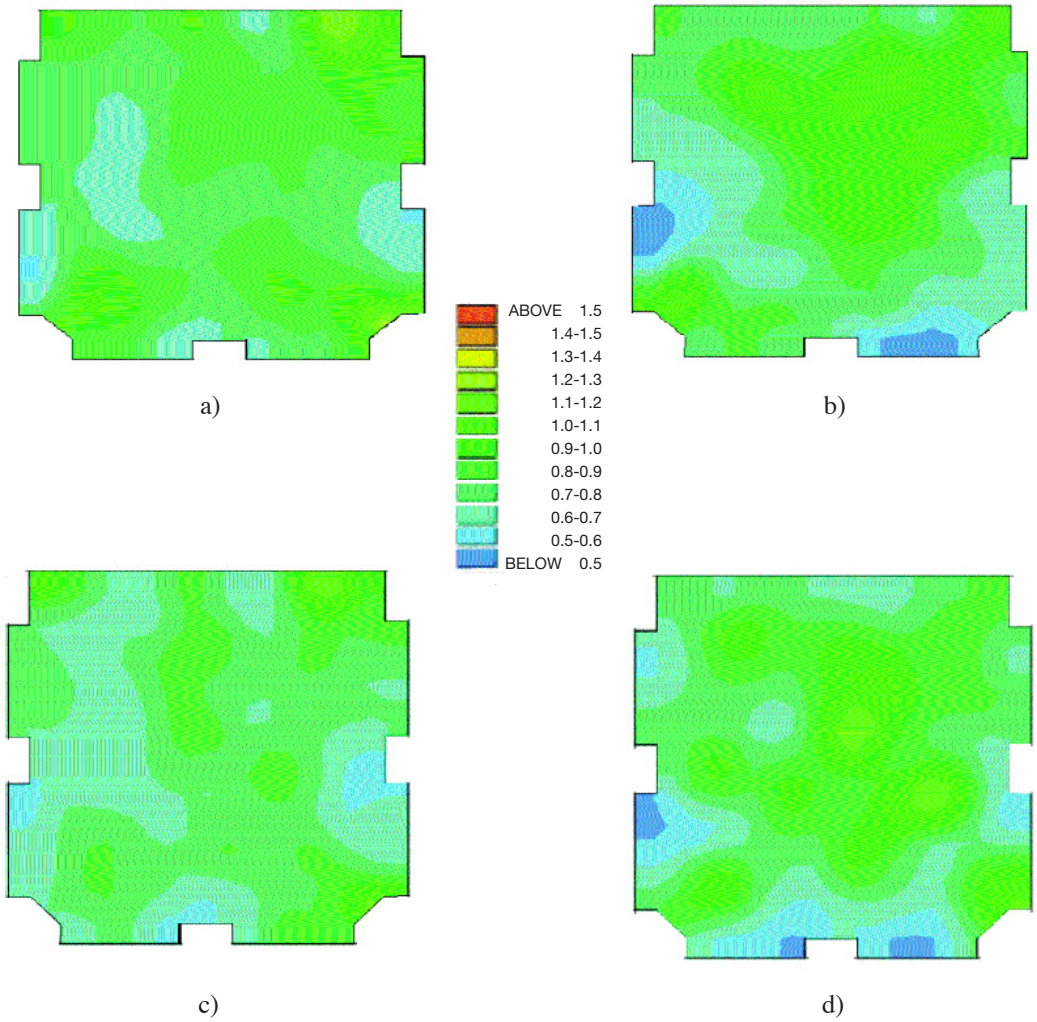

Fig. 10 - a) and b) field velocities of two sections of pillar D2 (S. Nicolò L'Arena) in the case of linear ray path approximation, c) and d) field velocities of two sections of pillar D2 in the case of ray tracing approximation (after Zanzi et al., 2001).

LTI interpolation alghorithm was used in the case of ray tracing approximation. In this case, isotropic material was considered. The complete processing and data acquisition of such survey is reported in the paper by Zanzi et al. (2001).

The results of sections 3 and 4 of pillar 2 are shown in Fig. 10. In the Figs. 10a and 10b the inversion results obtained with straight ray path approximation are shown, whilst in Figs. 10c and 10d the results are obtained with ray tracing. In this case, there is no difference between the two different approximations. This result is confirmed observing the values of data distance where the values are quite similar, even if, in the case of the straight ray, the values are lower. This is probably because there is not a high velocity contrast between the cells, in fact, excluding some superficial zones where the velocities are lower, the inner core seems to be quite homogeneous.

Also in this case, covariance matrices were calculated, the values of the main diagonal of the matrices confirm that the quality of the inversion is quite similar when comparing the two approximations even if the straight ray path approximation seems to be better (Fig. 11) where the UCM of section 3 is shown.

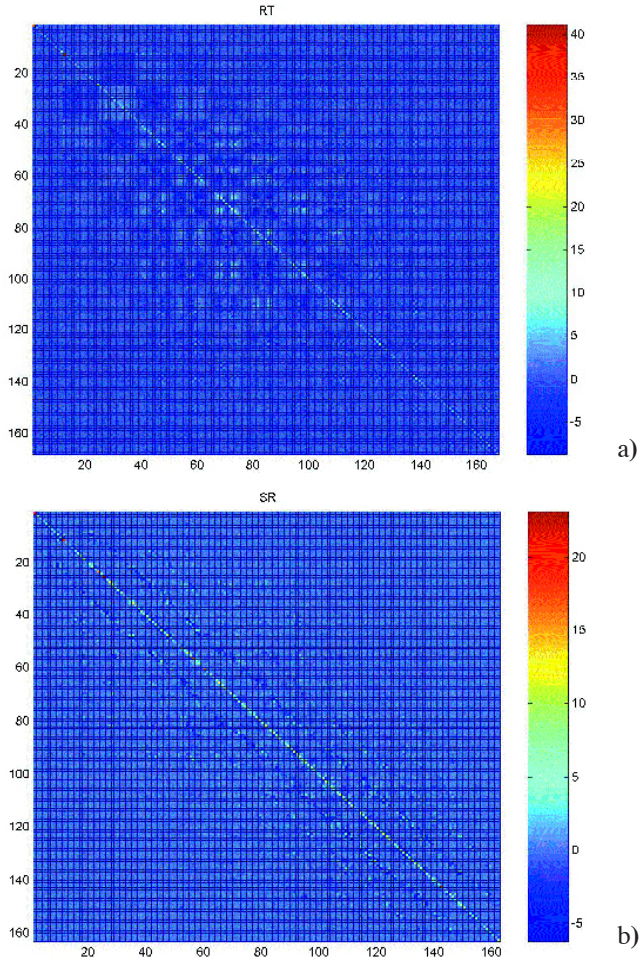

Fig. 11 - UCM of the last inversion in the case of ray tracing (a) and linear ray path (b).

5. Conclusions

Ray tracing is a useful tool to improve the quality of inversion results. The choice of the algorithm depends on the characteristics of the investigated soil and by the kind of survey. The use of ray tracing approximation does not seem to be, in any case, the best choice. In fact, in the case of homogeneous materials the straight ray path approximation could be preferred because it gives the same or even better results than ray tracing, considering that ray tracing is more time consuming. In the case of the anisotropic model it has to consider the components of the ray to understand the quality of the ray coverage. To analyse this parameter UCM is a very useful tool.

Acknowledgments. The author thanks Prof. M. Bernabini for the critical reading of the paper and the useful suggestions. Furthermore the author wishes to thank Prof. L. Zanzi and Prof. M. Lualdi who permitted us to present part of the results of a common work on the church of S. Nicolò all'Arena in Catania.

Appendix A

The main steps of the calculus of the traveltime between two grid points is summarised by the formulas indicated here with reference to Fig. 1A. *S* indicates the slowness of the considered

$$T_D = T_C + T_P, \tag{1A}$$

cell A and B are two grid points, C is the point where the minimum time is detected to travel in D.

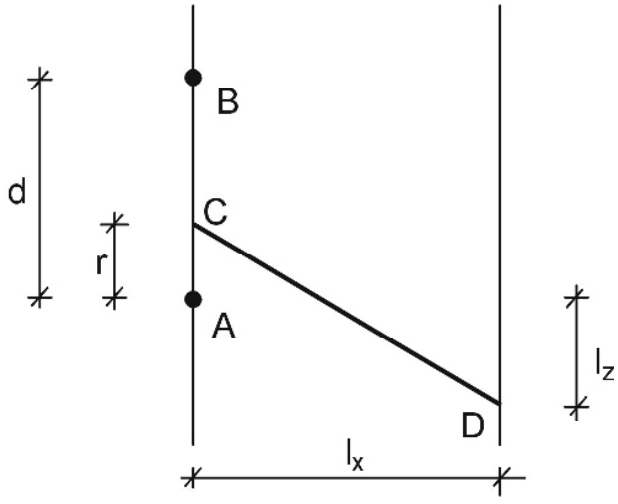

Fig. 1A - Sketch of a ray path that crosses segment AB at point C and reaches D in a cell for the case of elliptical anisotropic media.

$$T_P = S\sqrt{(1_Z + r)^2 + 1_X^2}\ , \tag{2A}$$

$$T_C = T_A - \frac{T_A - T_B}{d} r = T_A - \frac{\Delta T}{d} r. \tag{3A}$$

Then:

$$T_D = T_A - \frac{\Delta T}{d} r + S\sqrt{(1_z + r)^2 + 1_x^2}. \tag{4A}$$

If we differentiate Eq. (4A) with respect to *r* and solve for zero:

$$T_D^{min} = T_A + \frac{\Delta T}{d} 1_z + \frac{\sqrt{S^2 d^2 - \Delta T^2}}{d} 1_x. \tag{5A}$$

This is the minimum travel-time that we consider.

Appendix B

The time T_D, that the seismic ray needs to reach point D starting from source S, is given by the sum of two contributions:

a) the starting time $T_i = T_C$, during which the seismic ray travels from the source to point C; according to the LTI approximation, and is given by $T_C = \dfrac{T_A - T_B}{d} r$;

b) the traveltime $T_p = \sqrt{S_x^2\, 1_x^2 + S_z^2\, (1_z + r)^2}$ between points C and D, derived from Eq. (2A).

As $T_D = T_i + T_p$, we can write:

$$T_D = T_A - \frac{\Delta T}{d} r + \sqrt{S_x^2\, 1_x^2 + S_z^2\, (1_z + r)^2} \quad , \tag{1B}$$

where $\Delta T = T_A - T_B \geq 0$ (choosing A as the calculation point with the greater time); furthermore 1_z and r are computed starting from A with signs that correspond to the direction indicated in Fig. 1B.

To locate point C, we look for the value of r that minimises T_D with the condition $0 \leq r \leq d$ (only paths crossing the segment AB are considered).

Consider the case when point D is located above point B: as point C is moved toward B, T_i and T_p both decrease, so $r = d$ (and C = B). If point D is underneath point B, for $r > -1_z$ the time T_i decreases whilst the distance CD increases (consequently T_p too); thus, there exists a value of

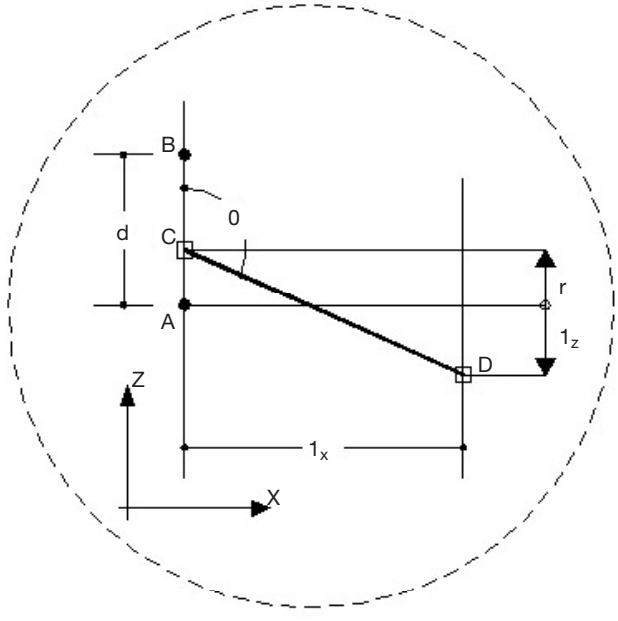

Fig. 1B - A sketch of a raypath that crosses segment AB at point C and reaches point D in a cell, for the case of an elliptical anisotropic medium.

r where $T_D = min$. In order to determine this point we differentiate Eq. (1B) with respect to r and solve for zero:

$$-\frac{\Delta T}{d}+\frac{S_z\,(1_z+r)}{\sqrt{S_x^2\,1_x^2+S_z^2\,(1_z+r)^2}}=0. \qquad (2B)$$

Considering that $(l_z + r) \geq 0$ and $\Delta T \geq 0$, from Eq. (2B):

$$r=\frac{S_x}{S_z}\frac{\Delta T 1_x}{\sqrt{S_z^2\,d^2-\Delta T^2}}-1_z. \qquad (3B)$$

Inserting Eq. (4A) into Eq. (2A) yields the minimum traveltime to point D:

$$T_D=T_A+\frac{\Delta T}{d}\,1_z+\frac{S_x}{S_z}\,\frac{\sqrt{S_z^2\,d^2-\Delta T^2}}{d}1_x. \qquad (4B)$$

As shown in Fig. 2B, where the trend of the sign of the first derivative of the function $T_D\,(r)$ is drawn, the position of point C depends on the value of ΔT. In fact, from Eq. (3B) we have:

$r \geq 0$ if $\Delta T \geq \dfrac{S_z^2\,d1_z}{\sqrt{S_x^2\,1_x^2+S_z^2\,1_z^2}}=\Delta T_{min}$,

$r \leq$ d if $\Delta T \leq \dfrac{S_z^2\,d\,(1_z+d)}{\sqrt{S_x^2\,1_x^2+S_z^2\,(1_z+d)^2}}=\Delta T_{max}$.

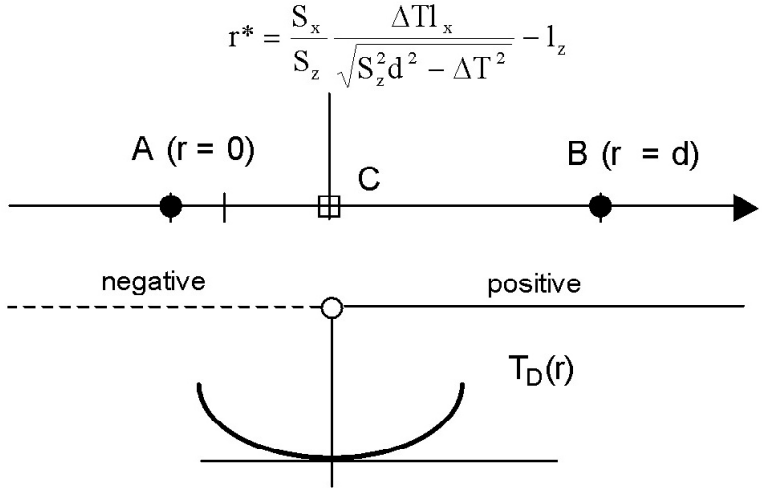

Fig. 2B - The pattern of the first derivative of *TD* (*r*): the location of point C depends on the value of (*T*).

Therefore, before using Eqs. (3B) and (4B) it is necessary to calculate ΔT and compare it with ΔT_{min} and ΔT_{max} following the procedure:

1) If $\Delta T \leq \Delta T_{min}$ then $r = 0$ and C = A,

2) If $\Delta T \geq \Delta T_{max}$ then $r = d$ and C = B,

3) If $\Delta T_{min} < \Delta T < \Delta T_{max}$ then $0 < r < d$ and T_D and r are given by Eqs. (4B) and (3B).

This procedure is valid also in the case of $l_z < -d$ (point D above point B); in fact, in this case $\Delta T_{max} < 0$ and consequently $r = d$. Note that the expressions ΔT_{min} and ΔT_{max} are written differently from the Asakawa and Kawanaka (1993) formulation, but are equivalent if the condition on the sign of ΔT is valid. This means that for the starting point we choose A, i.e. the one where the time is the greatest.

Refraction with critical angle

The LTI method assumes a straight ray path approximation within each cell. This means that when the ray calculus reaches a point at the source cell boundary it can be joined to the source by a segment. However, when the reached point coincides with a corner of the cell (Fig. 3B) it is necessary to assess whether or not it is the head wave that gives the first arrival at that point. With reference to Fig. 3B we can write:

$$T_p = \sqrt{\frac{h^2}{V_{1z}^2} + \frac{x^2}{V_{1z}^2}} + \frac{b - x}{V_{2x}}. \tag{5B}$$

Given the condition of minimum traveltime we have:

$$\frac{dT_p}{dx} = \frac{\frac{x}{V_{1x}^2}}{\sqrt{\frac{h^2}{V_{1z}^2} + \frac{x^2}{V_{1x}^2}}} - \frac{1}{V_{2x}} = 0.$$

From which, if $V_{2x} > V_{1x}$:

$$x = \frac{V_{1x}^2 h}{V_{1z}\sqrt{V_{2x}^2 - V_{1x}^2}}. \tag{6B}$$

Because:

$$x^2 = (x^2 + h^2)\, sin^2\, \theta_c,$$

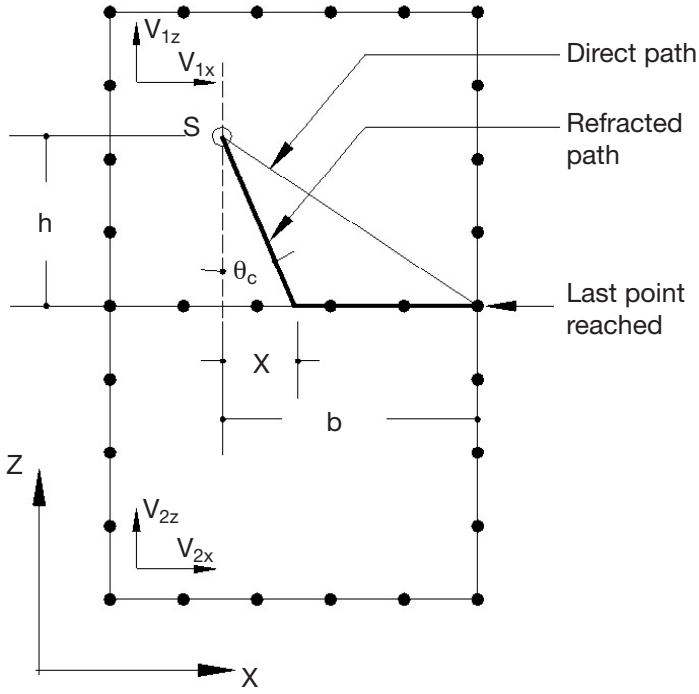

Fig. 3B - Refraction of a critical angle (c) in an elliptical anisotropic layered medium.

using Eq. (6B) we get:

$$sin^2 \theta_c = \frac{V_{1x}^4}{V_{1x}^4 + V_{1y}^2 (V_{2x}^2 - V_{1x}^2)} \qquad \text{(7B)}$$

Eq. (7B) represents a particular case (critical angle of incidence) of the formula given by Levin (1978).

References

Aki K. and Lee W.H.K.; 1976: *Determination of three-dimensional velocity anomalies under a seismic array using first P arrival times from local earthquakes, I, a homogeneous initial model*. Journal of Geophys. Res., **81**, 4381-4399.

Asakawa E. and Kawanaka T.; 1993: *Seismic ray tracing using linear travel time interpolation*. Geophys. Pros., **41**, 99-111.

Bois P., La Porte M., Lavargne M. and Thomas G.; 1971: *Essai de determination automatique des vitesses sismique par mesures entre puits*. Geophys. Pros., **19**, 42, 83.

Cardarelli E.; 2000: *Seismic transmission tomography: determination of the elastic properties of buiding structures (some examples)*. Annali di Geofisica, **43**, 1075-1089.

Cardarelli E. and Cerreto A.; 2002: *Ray tracing in elliptical anisotropic media using LTI method applied to traveltime seismic tomography*. Geophys. Pros., **50**, 55-72.

Cardarelli E. and de Nardis R.; 2001: *Seismic refraction, isotropic and anisotropic seismic tomography on an ancient monument (Antonino and Faustina temple 141 A.D.)*. Geophys. Pros., **49**, 228-240.

Cerveny V.; 1972: *Seismic ray and ray intensities in inhomogeneous anisotropic media*. Geophys. J. Astr. Soc., **29**, 1-13.

Cerveny V.; 1987: *Ray tracing algorithms in three-dimensional laterally varying layered structures*. In: Nolet G. (ed), Seismic Tomography, D. Reidel Pub. Co., Boston (Mass.) pp. 99-133.

Cerveny V., Molotkov I.A. and Psencik I.; 1977: *Ray method in seismology* Univerzita Karlova, Praha, 214 pp.

Chapman C.H. and Pratt R.G.; 1992: *Travel-time tomography in anisotropic media*. Theory, Geophys. J. Int., **109**, 1-19.

Faria E. and Stoffa P.; 1994: *Traveltime computation in transversely isotropic media*. Geophysics, **59**, 272-281.

Levin F.K.; 1978: *The reflection, refraction and diffraction of waves in media with an elliptical velocity dependence*. Geophysics, **43**, 528-537.

Li X.G. and Ulrych T.J.; 1993: *LTI formulations and application to curved wave fronts*. J. Seismic Expl., **2**, 239-246.

Lytle R.J. and Dines K.; 1980: *Iterative ray tracing between boreholes for underground image reconstruction IEEE Transaction on Geoscience and Remote Sensing*. **18**, 234 -239.

Julian B.R. and Gubbins D.; 1977: *Three-dimensional seismic raytracing*. J. Geoph., **43**, 95-113.

Matsuoka T. and Ezaka T.; 1992: *Ray tracing using reciprocity.* Geophysics, **57**, 326-333.

Menke W.; 1989: *Geophysical data analysis: Discrete Inverse Theory*. International Geophysics Series, 289 pp.

Michelena R.J., Muir F. and Harris J.M.; 1993: *Anisotropic traveltime tomography.* Geophys. Pros., **41**, 381-412.

Moser T.J.; 1991: *Shortest path calculation of seismic ray.* Geophysics, **56**, 59-67.

Postma G.W.; 1955: *Wave propagation in a stratified medium*. Geophysics, **20**, 780-806.

Pratt R.G. and Chapman C.H.; 1992: *Travel-time tomography in anisotropic media 2*. Appl. Geophys. J. Int., **109**, 20-37.

Press H.V., Tenkolsky S.A., Vetterling W.T. and Flannery B.P.; 1992: *Numerical Recipes in Fortran*. Cambridge University Press, 2nd Edition, 933 pp.

Saito H.; 1989: *Traveltimes and raypaths of first arrival seismic waves: computation method based on Hhuyghen's principle*. In: SEG (ed), Fifty-ninth Annual International Meeting & Exposition, Expanded Abstracts of the Technical Program with Authors' Biographies, Dallas, pp. 244-247.

Saito H.; 1990: *3-D ray tracing method based on Huyghens' principle*. In: SEG (ed), Sixtieh Annual International Meeting & Exposition, Expanded Abstracts of the Technical Program with Authors' Biographies, San Francisco, pp. 1024-1027.

Vidale J.; 1988: *Finite difference calculation of traveltimes*. Bull. Seis. Soc. Am., **78**, 2062-2076.

Vidale J.; 1990: *Finite-difference calculation of traveltimes in three dimensions*. Geophysics, **55**, 521-526.

Wesson R.L.; 1971: *Travel-time inversion for laterally inhomogeneous crustal velocity models*. Bull. Seismol. Soc. Am., **61**, 729-746.

Zanzi L., Cardarelli E. and Lualdi M.; 2001: *Velocity and absorption analysis from tomographic sonic experiments on ancient stone piers*. In: Proc. 63th Conference of EAEG, Extended Abstract, Amsterdam, paper N 32.